Supporting Information:

Atomically tailoring vacancy defects in $FeF_{2.2}(OH)_{0.8}$ toward ultra-high rate and long-life Li/Na-ion batteries

Qun Wang,[ab] Zhenhua Yang, *[ab] Hanghui Liu,[ab] Xianyou Wang,[c] and Xingqiang Shi[d]

[a]*Key Laboratory of Materials Design and Preparation Technology of Hunan Province, School of Materials Science and Engineering, Xiangtan University, Xiangtan 411105, Hunan, China.*

[b]*Key Laboratory of Low Dimensional Materials & Application Technology (Ministry of Education), School of Materials Science and Engineering, Xiangtan University, Xiangtan 411105, Hunan, China*

[c]*National Local Joint Engineering Laboratory for Key Materials of New Energy Storage Battery, National Base for International Science & Technology Cooperation, Hunan Province Key Laboratory of Electrochemical Energy Storage & Conversion, School of Chemistry, Xiangtan University, Xiangtan 411105, Hunan, China*

[d]*Department of Physics, Southern University of Science and Technology, Shenzhen 518055, China.*

1. Thermodynamic stability of $FeF_{2.2}(OH)_{0.8}$

Chemical potential has a close relationship with the formation enthalpy of vacancy defects in solids. And it is an important parameter for defining the thermodynamic stability diagram. The individual chemical potentials (μ_i) of isolated atoms are usually lower than the atomic chemical potentials of stable elements in the same substance.[1] Here, $\mu_i = \mu_i^{solid/gas} + \Delta\mu_i$ (where the $\mu_i^{solid/gas}$ means the chemical potential of the standard reference state equivalent to the total energy per atom, and the $\Delta\mu_i$ the denotes relative chemical potential). In order to maintain stability of $FeF_{2.2}(OH)_{0.8}$, $\Delta\mu_{Fe}$, $\Delta\mu_F$, $\Delta\mu_H$ and $\Delta\mu_O$ must satisfy following

*Corresponding authors. Address: Key Laboratory of Materials Design and Preparation Technology of Hunan Province, School of Materials Science and Engineering, Xiangtan University, Xiangtan 411105, Hunan, China.

E-mail addresses: yangzhenhua@xtu.edu.cn (Zhenhua Yang).

relationships:

$$\Delta\mu_F \leq 0, \Delta\mu_{Fe} \leq 0, \Delta\mu_H \leq 0, \Delta\mu_O \leq 0 \quad (1)$$

$$2.2\Delta\mu_F + \Delta\mu_{Fe} + 0.8\Delta\mu_H + 0.8\Delta\mu_O = \Delta H_f^{FeF_{2.2}(OH)_{0.8}} \quad (2)$$

Where $\Delta H_f^{FeF_{2.2}(OH)_{0.8}}$ is the formation enthalpy of $FeF_{2.2}(OH)_{0.8}$. Besides, $\Delta\mu_{Fe}$, $\Delta\mu_F$, $\Delta\mu_H$ and $\Delta\mu_O$ must also be further limited to prevent precipatation processes of the possible competing phases, which implies that

$$3\Delta\mu_F + \Delta\mu_{Fe} \leq \Delta H_f^{FeF_3} \quad (3)$$

$$2\Delta\mu_F + \Delta\mu_{Fe} \leq \Delta H_f^{FeF_2} \quad (4)$$

$$\Delta\mu_{Fe} + \Delta\mu_o \leq \Delta H_f^{FeO} \quad (5)$$

$$2\Delta\mu_{Fe} + 3\Delta\mu_o \leq \Delta H_f^{Fe_2O_3} \quad (6)$$

$$3\Delta\mu_{Fe} + 4\Delta\mu_o \leq \Delta H_f^{Fe_3O_4} \quad (7)$$

$$2\Delta\mu_H + \Delta\mu_O \leq \Delta H_f^{H_2O} \quad (8)$$

The calculated formation enthalpy can be obtained from the following equations (see **Table S1**)

$$\Delta H_f^{FeF_3} = E_{tot}^{FeF_3} - E_{tot}^{Fe} - \frac{3}{2}E_{tot}^{F_2} \quad (9)$$

$$\Delta H_f^{FeF_2} = E_{tot}^{FeF_2} - E_{tot}^{Fe} - E_{tot}^{F_2} \quad (10)$$

$$\Delta H_f^{FeO} = E_{tot}^{FeO} - E_{tot}^{Fe} - \frac{1}{2}E_{tot}^{O_2} \quad (11)$$

$$\Delta H_f^{Fe_2O_3} = E_{tot}^{Fe_2O_3} - 2E_{tot}^{Fe} - \frac{3}{2}E_{tot}^{O_2} \quad (12)$$

$$\Delta H_f^{Fe_3O_4} = E_{tot}^{Fe_3O_4} - 3E_{tot}^{Fe} - 2E_{tot}^{O_2} \quad (13)$$

$$\Delta H_f^{H_2O} = E_{tot}^{H_2O} - E_{tot}^{H_2} - \frac{1}{2}E_{tot}^{O_2} \quad (14)$$

where E_{tot} is the total energies of the bulk unit cells. To obtain the total energies of H_2, O_2

and F_2, spin-polarized calculations are carried out. And two H, O and F atoms are placed together at the distance of 0.75 Å, 1.21 Å and 1.42 Å in a cubic box with periodic conditions and 15 Å lattice constant. The Calculated values of formation enthalpy of binary compounds were shown in **Table S1**, which shows good agreement with their experimental data.

Table S1. The calculated and experimental values of formation enthalpy of binary compounds.

Compounds	Calculated value (eV)	Experimental value (eV)
$FeF_{2.2}(OH)_{0.8}$	-11.61	
FeF_3	-10.10	-10.80[2]
FeF_2	-7.69	-7.31[2]
FeO	-2.92	-2.82[2]
Fe_2O_3	-8.50	-8.49[2]
Fe_3O_4	-11.25	-11.55[2]
H_2O	-2.43	-2.51[2, 3]

2. The vacancy defect structure of $FeF_{2.2}(OH)_{0.8}$

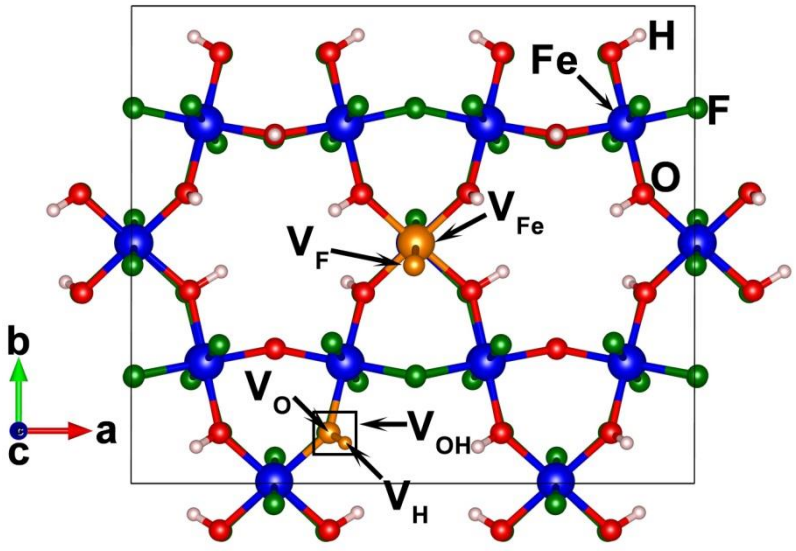

Fig. S1 The vacancy defect structure of $FeF_{2.2}(OH)_{0.8}$.

Fig. S1 displays the vacancy defect structure (V_F , V_{Fe} , V_O , V_H and V_{OH}) of $FeF_{2.2}(OH)_{0.8}$. **Fig. S2a** shows the different atomic configurations of $FeF_{2.2}(OH)_{0.8}$ with neutral

OH vacancy (V_{OH}^{0}). Six different vacancy defect positions were considered and they were labeled as a, b, c, d, e and f, respectively. The relative energies of these six structures were calculated, as shown in **Fig. S2b.** It is found that the neutral OH vacancy (V_{OH}^{0}) prefers to form at site-c due to the lowest energy.

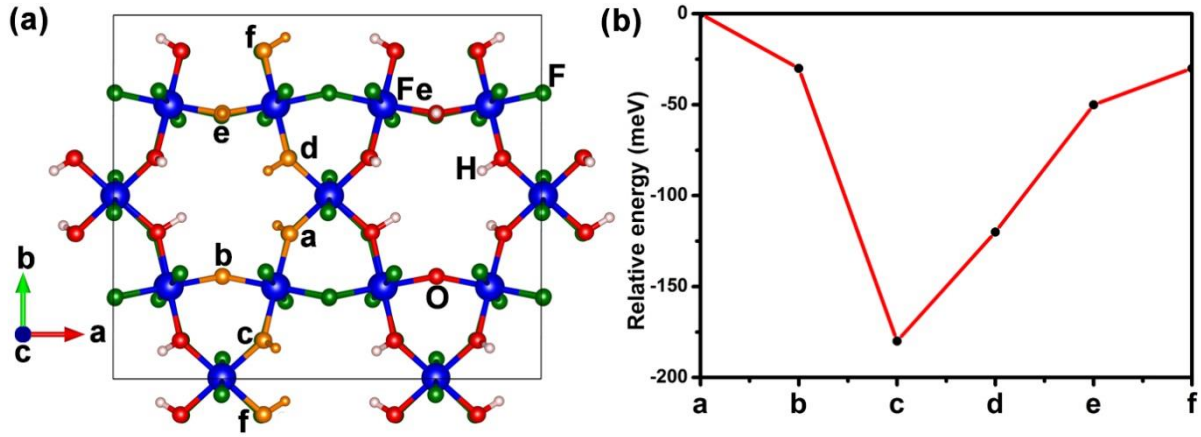

Fig. S2 (a) The different atomic configurations of $FeF_{2.2}(OH)_{0.8}$ with neutral OH vacancy (V_{OH}^{0}). (b) Corresponding relative energy of these six structures with neutral OH vacancy (V_{OH}^{0}).

3. The close relationship between oxygen pressure and temperature

$\Delta\mu_{O}$ has close relationship with temperature (T) and oxygen pressure (P_{O_2}), and it can be expressed as:[4]

$$
\begin{aligned}
\Delta\mu_{O}(T, P_{O_2}) &= \mu_{O}(T, P) - \frac{E_{O_2}}{2} \\
&= \frac{1}{2}(\mu_{O_2}^{gas}(T, P) - E_{O_2}) \\
&= \frac{1}{2}[h_{O_2}^{0} - T^{0}S_{O_2}^{0} + \Delta G_{O_2}^{gas}(T, P^{0}) + kT\ln(\frac{P_{O_2}}{P^{0}}) - E_{O_2}] \\
&= \frac{1}{2}[\Delta G_{O_2}^{gas}(T, P^{0}) + kT\ln(\frac{P_{O_2}}{P^{0}})] + \frac{1}{2}(h_{O_2}^{0} - E_{O_2} - T^{0}S_{O_2}^{0}) \\
&= \frac{1}{2}[\Delta G_{O_2}^{gas}(T, P^{0}) + kT\ln(\frac{P_{O_2}}{P^{0}})] + \delta\mu_{O}^{0}
\end{aligned}
\qquad (15)
$$

Where $\delta\mu_O^0$ = 0.44 eV is a correction which is agreement with experimental and quantum mechanical computations.[4, 5] Under the pressure of P^0 (1 atm), $\Delta G_{O_2}^{gas}(T, P^0)$ is the relative oxygen Gibbs free energy at different temperature (T) with respect to the Gibbs free energy at T^0 = 298.15 K:

$$\Delta G_{O_2}^{gas}(T, P^0) = G_{O_2}^{gas}(T, P^0) - G_{O_2}^{gas}(T^0, P^0) \quad (16)$$

And $\Delta G_{O_2}^{gas}(T, P^0)$ at different temperature (T) can be calculated and presented in **Table S2.**[4]

Table S2. Variations in the Gibbs free energy for gaseous oxygen at standard pressure (P^0 = 1atm) with respect to its value at 0 K.[4]

T/K	$\Delta G_{O_2}^{gas}(T, P^0)$ (eV)	T/K	$\Delta G_{O_2}^{gas}(T, P^0)$ (eV)
200	-0.17	700	-0.73
298.15	-0.27	800	-0.85
300	-0.27	900	-0.97
400	-0.38	1000	-1.10
500	-0.50	1100	-1.23
600	-0.61	1200	-1.36

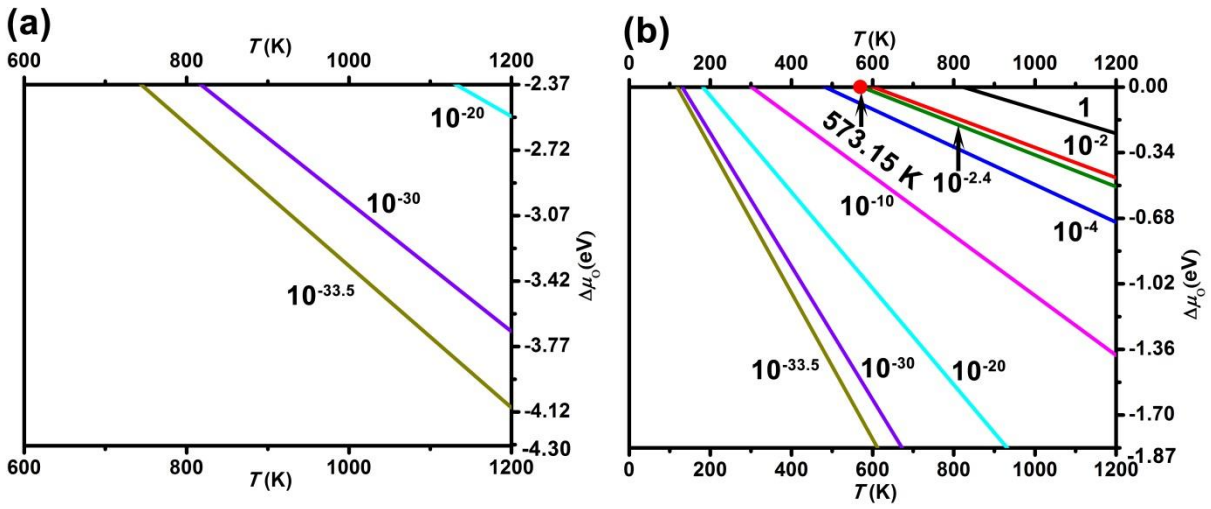

Fig. S3 The close relationship among $\Delta\mu_O$, oxygen pressure (P_{O_2}) and temperature (T) under (a) hydrogen-rich and (b) hydrogen-poor conditions.

4. The formation energy of charged vacancy under the H-rich and H-poor growth conditions

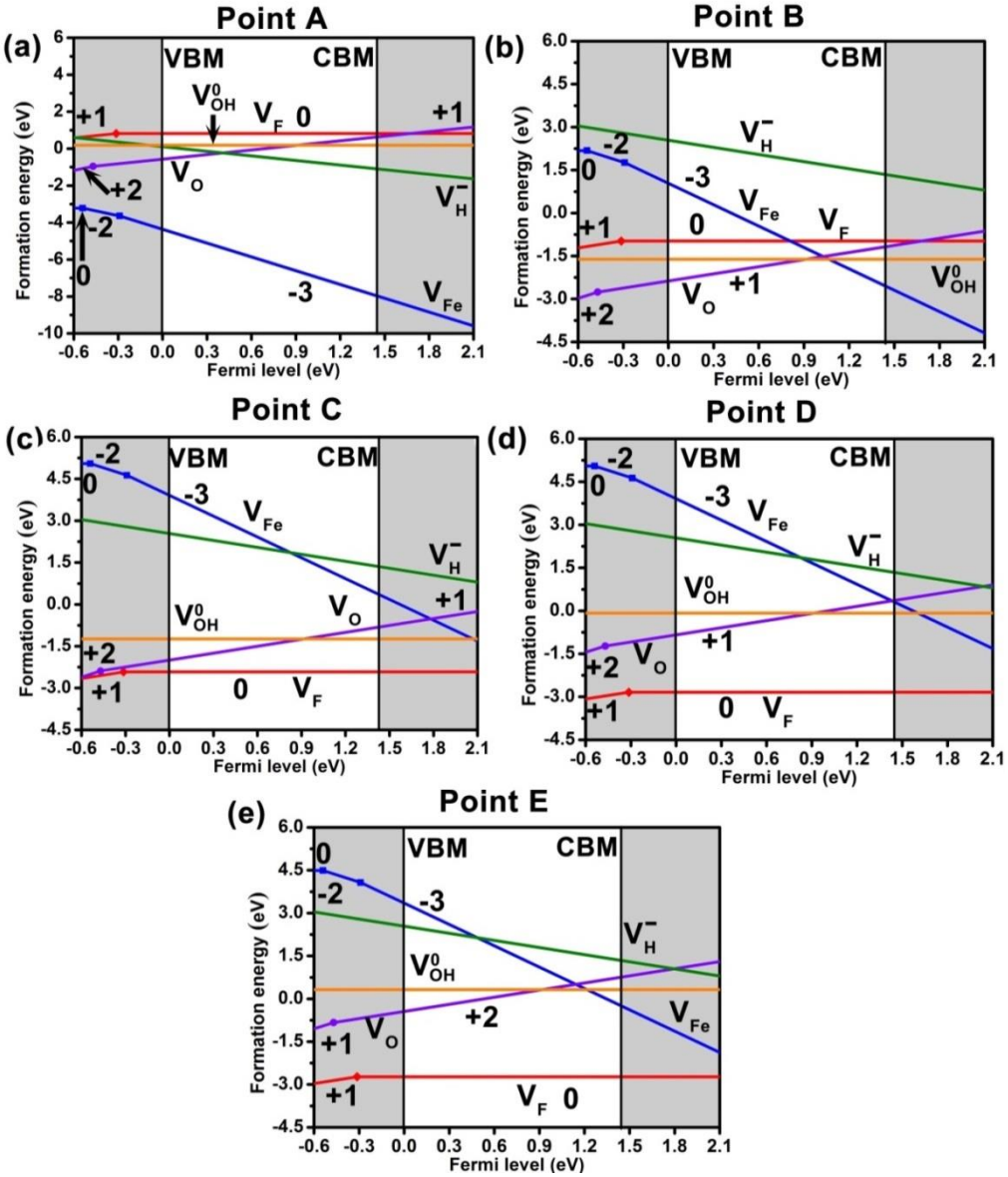

Fig. S4 The formation energy of charged vacancy as a function of the Fermi energy under the H-rich growth conditions. (a) point A ($\Delta\mu_F$ = -0.61 eV, $\Delta\mu_{Fe}$ = -8.27 eV, $\Delta\mu_O$ = -2.50 eV, $\Delta\mu_H$ = 0 eV); (b) point B ($\Delta\mu_F$ = -2.41 eV, $\Delta\mu_{Fe}$ = -2.87 eV, $\Delta\mu_O$ = -4.30 eV, $\Delta\mu_H$ = 0 eV); (c) point C ($\Delta\mu_F$ = -3.85 eV, $\Delta\mu_{Fe}$ = 0 eV, $\Delta\mu_O$ = -3.93 eV, $\Delta\mu_H$ = 0 eV); (d) point D ($\Delta\mu_F$ = -4.27 eV, $\Delta\mu_{Fe}$ = 0 eV, $\Delta\mu_O$ = -2.77 eV, $\Delta\mu_H$ = 0 eV); (e) point E ($\Delta\mu_F$ = -4.16 eV, $\Delta\mu_{Fe}$ = -0.56 eV, $\Delta\mu_O$ = -2.37 eV, $\Delta\mu_H$ = 0 eV).

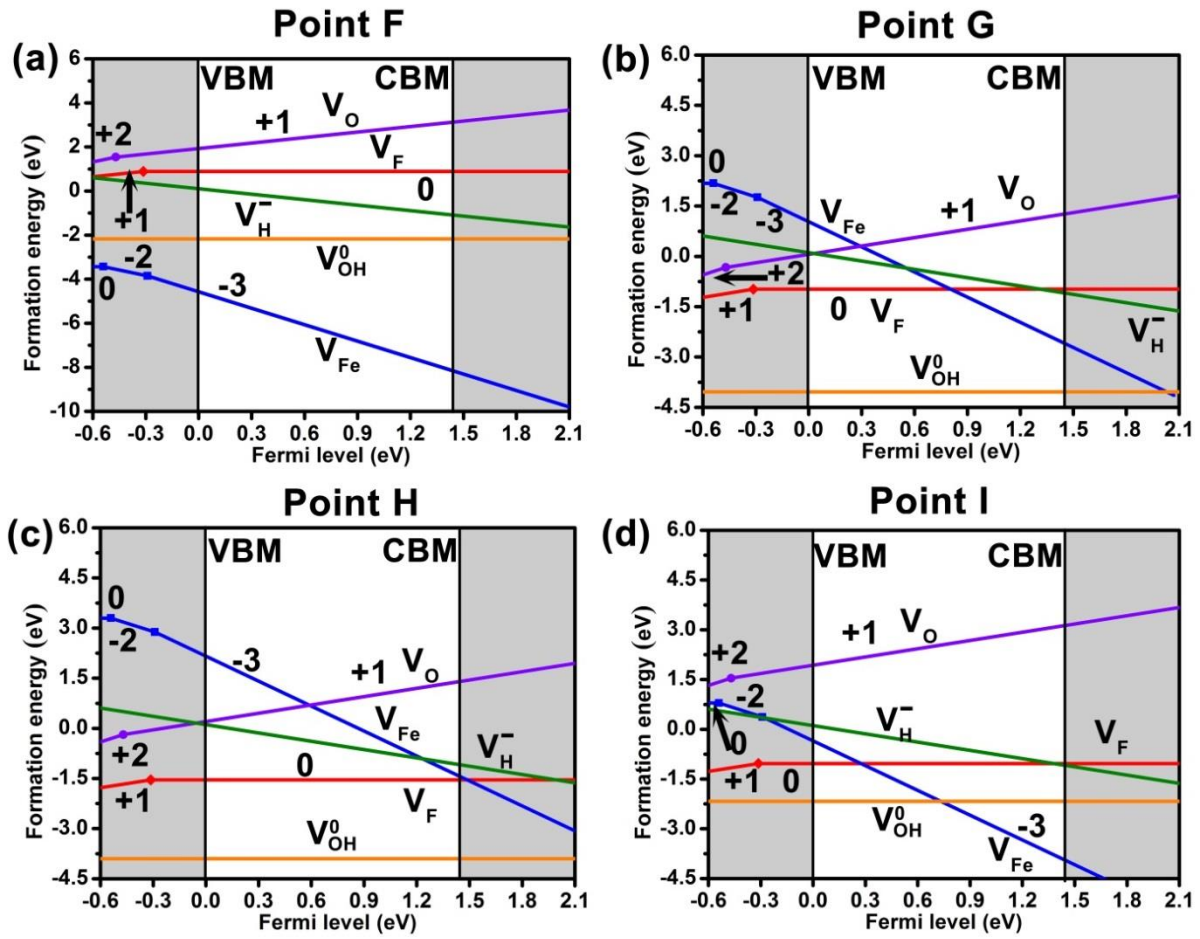

Fig. S5 The formation energy of charged vacancy as a function of the Fermi energy under the H-poor growth conditions. (a) F ($\Delta\mu_F$ = -0.54 eV, $\Delta\mu_{Fe}$ = -8.48 eV, $\Delta\mu_O$ = 0 eV, $\Delta\mu_H$ = -2.43 eV); (b) G ($\Delta\mu_F$ = -2.41 eV, $\Delta\mu_{Fe}$ = -2.87 eV, $\Delta\mu_O$ = -1.87 eV, $\Delta\mu_H$ = -2.43 eV); (c) H ($\Delta\mu_F$ = -2.97 eV, $\Delta\mu_{Fe}$ = -1.75 eV, $\Delta\mu_O$ = -1.73 eV, $\Delta\mu_H$ = -2.43 eV) ; (d) I ($\Delta\mu_F$ = -2.46 eV, $\Delta\mu_{Fe}$ = -4.26 eV, $\Delta\mu_O$ = 0 eV, $\Delta\mu_H$ = -2.43 eV).

5. Sections of diffusion channel of $FeF_{2.2}(OH)_{0.8}$ and $FeF_{2.2}(OH)_{0.64}O_{0.08}\square_{0.08}$

In order to clarify clearly the detailed channel size before and after vacancy formation, we provided the sections of diffusion channel of $FeF_{2.2}(OH)_{0.8}$ and $FeF_{2.2}(OH)_{0.64}O_{0.08}\square_{0.08}$, respectively. We calculated their area (see **Fig. S6**). It is noted that area of $FeF_{2.2}(OH)_{0.64}O_{0.08}\square_{0.08}$ is larger than that of $FeF_{2.2}(OH)_{0.8}$ (34.90 $Å^2$ *vs*.31.53 $Å^2$).

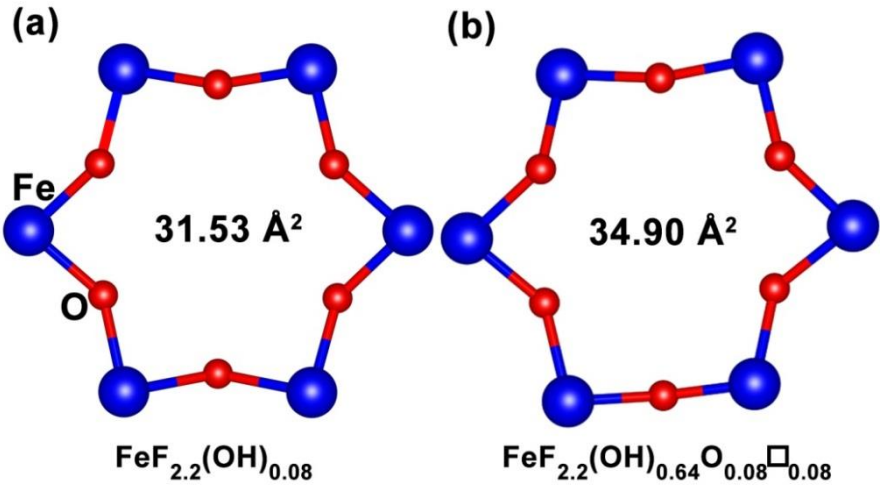

Fig. S6 The cross-sectional area of diffusion channel in (a) $FeF_{2.2}(OH)_{0.8}$ (31.53Å^2) and (b) $FeF_{2.2}(OH)_{0.64}O_{0.08}\square_{0.08}$ (34.90Å^2).

6. The Electronic Structure of $FeF_{2.2}(OH)_{0.8}$ and $FeF_{2.2}(OH)_{0.64}O_{0.08}\square_{0.08}$

To further investigate the electronic structure of $FeF_{2.2}(OH)_{0.8}$ and $FeF_{2.2}(OH)_{0.64}O_{0.08}\square_{0.08}$, we investigated the local structure and density of states (DOS) of $FeF_{2.2}(OH)_{0.8}$ and $FeF_{2.2}(OH)_{0.64}O_{0.08}\square_{0.08}$, which were shown in **Fig.S7-S10**, respectively. It can be seen from **Fig. S9**, there are four types of Fe atomic configurations (Fe1, Fe2-Fe5, Fe6 and Fe7-Fe10), and the band gap is mainly contributed by Fe7-Fe10. With OH group is introduced, there are six types of Fe atomic configurations (Fe1, Fe2-Fe3, Fe4-Fe5, Fe6, Fe7-Fe8 and Fe9-F10). While the band gap is mainly contributed by Fe9-Fe10,and conduction band of Fe9-Fe10 moves toward the low-energy direction.

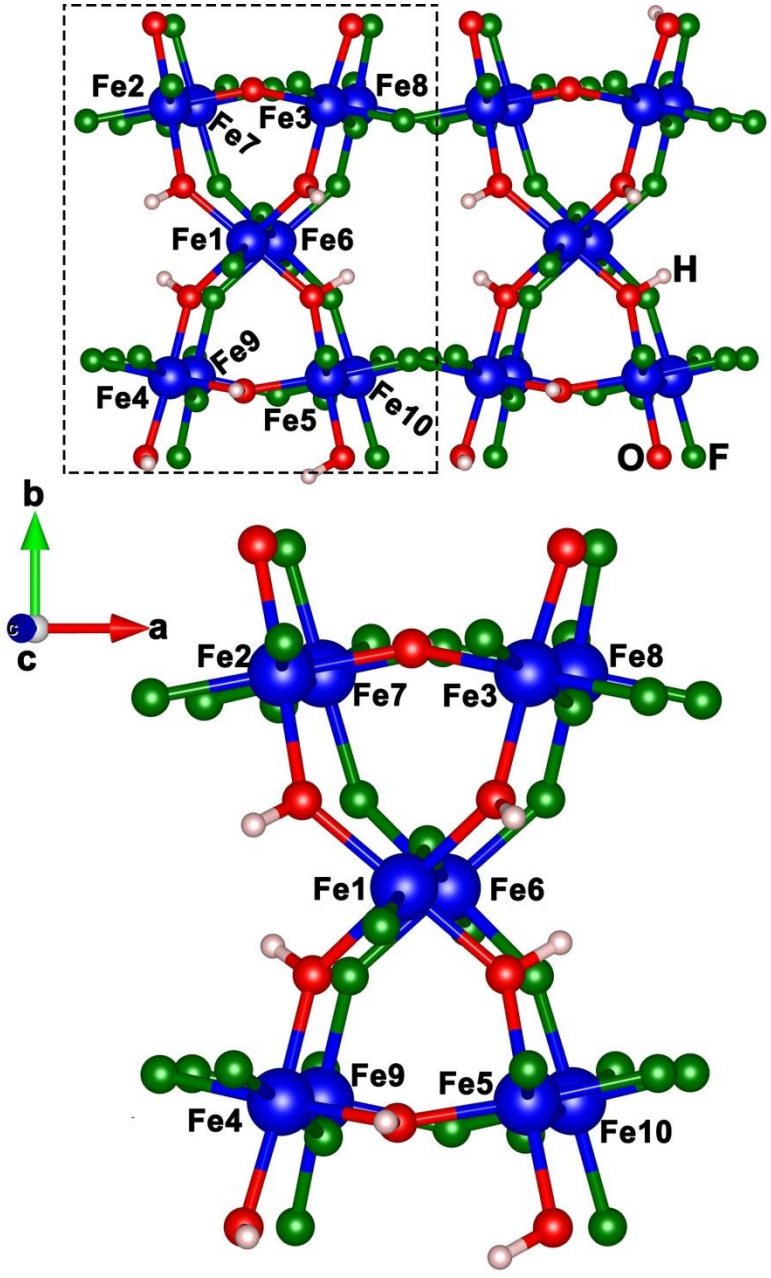

Fig. S7 The local structure of $FeF_{2.2}(OH)_{0.8}$.

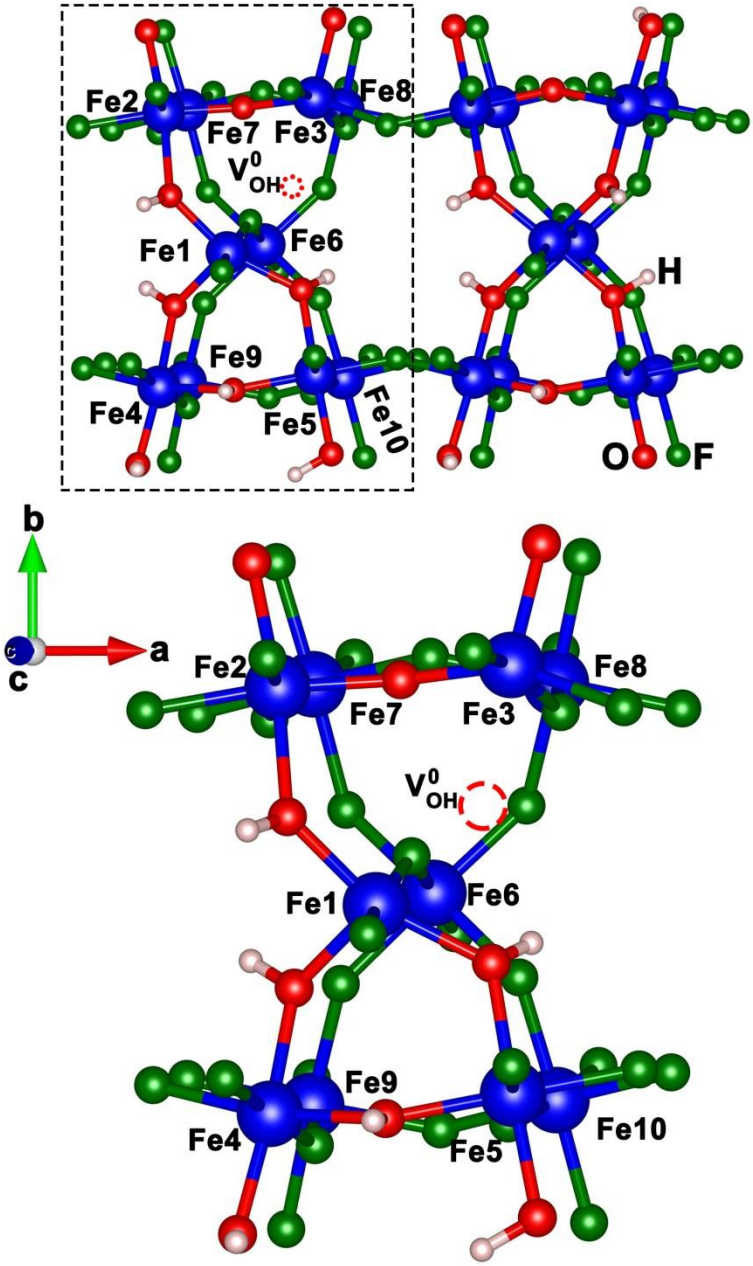

Fig. S8 The local structure of $FeF_{2.2}(OH)_{0.64}O_{0.08}\square_{0.08}$.

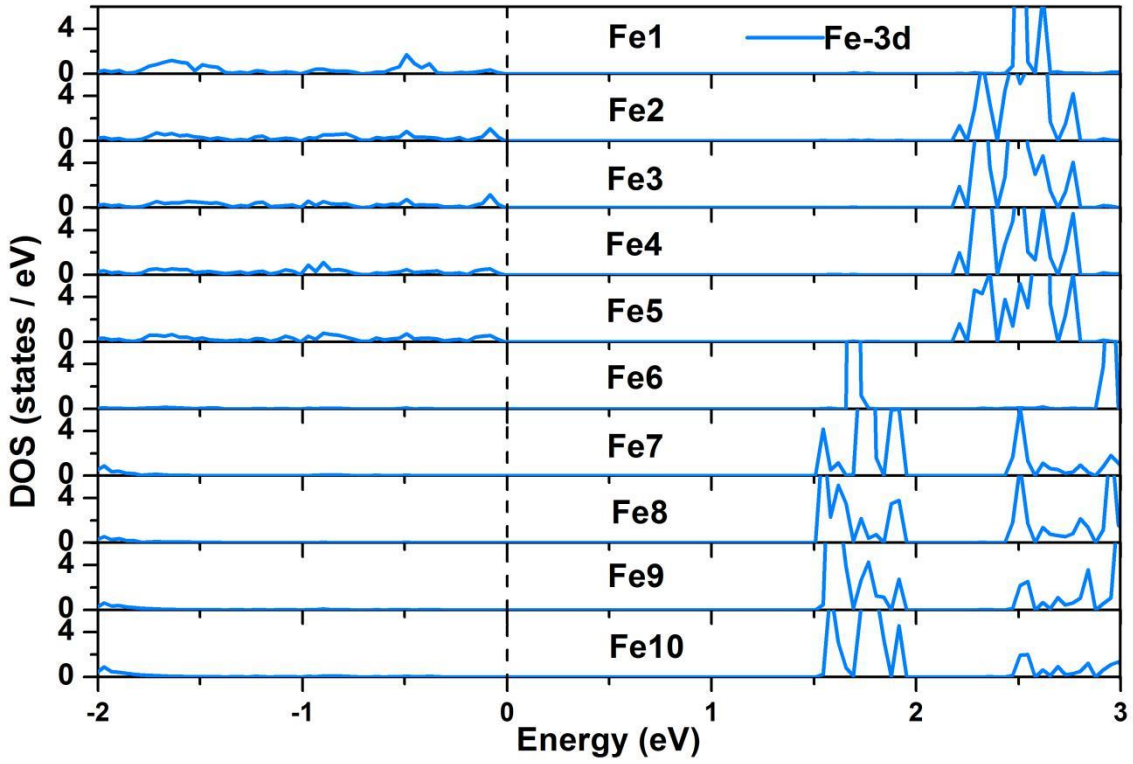

Fig. S9 Density of states of Fe atoms in the $FeF_{2.2}(OH)_{0.8}$.

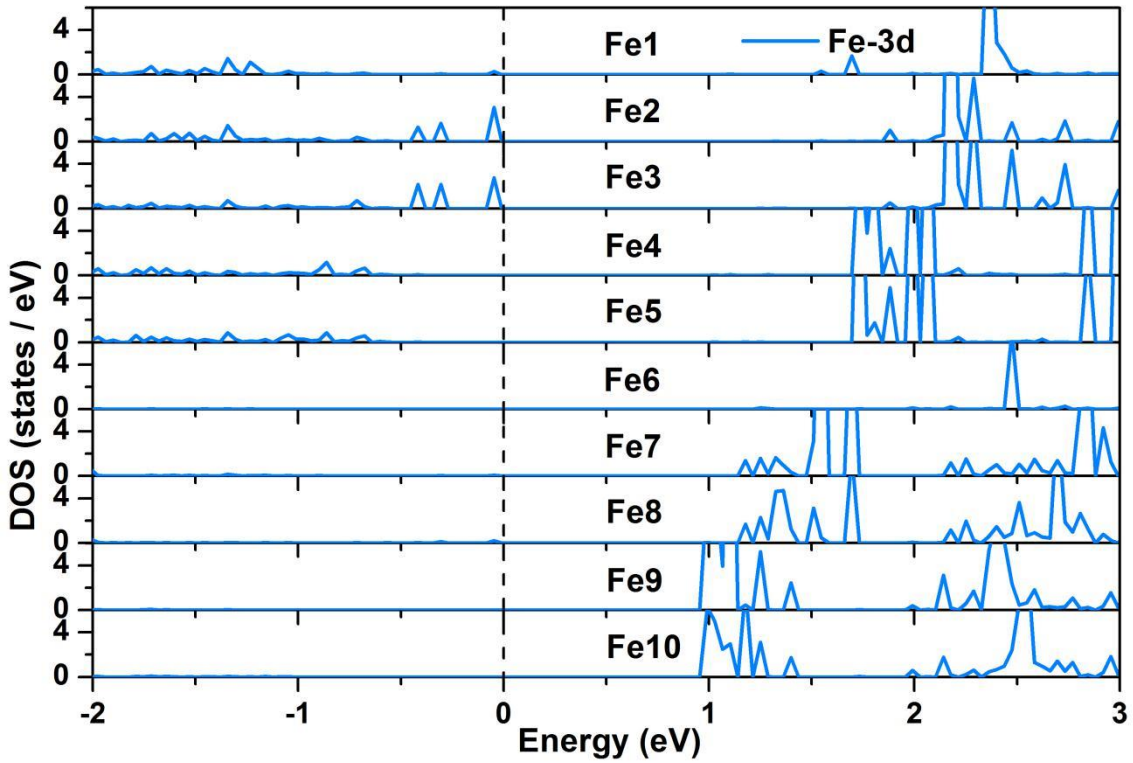

Fig. S10 Density of states of Fe atoms in the $FeF_{2.2}(OH)_{0.64}O_{0.08}\square_{0.08}$.

7. Li/Na optimal occupation sites in $FeF_{2.2}(OH)_{0.8}$ and $FeF_{2.2}(OH)_{0.64}O_{0.08}\square_{0.08}$

In order to explore the Li/Na optimal occupation sites in $FeF_{2.2}(OH)_{0.8}$ and $FeF_{2.2}(OH)_{0.64}O_{0.08}\square_{0.08}$, we considered eight possible initial sites occupied by Li or Na. And they are labeled as a, b, c, d, e, f, g and h, respectively. (see **Fig. S11** and **Fig. S12**)

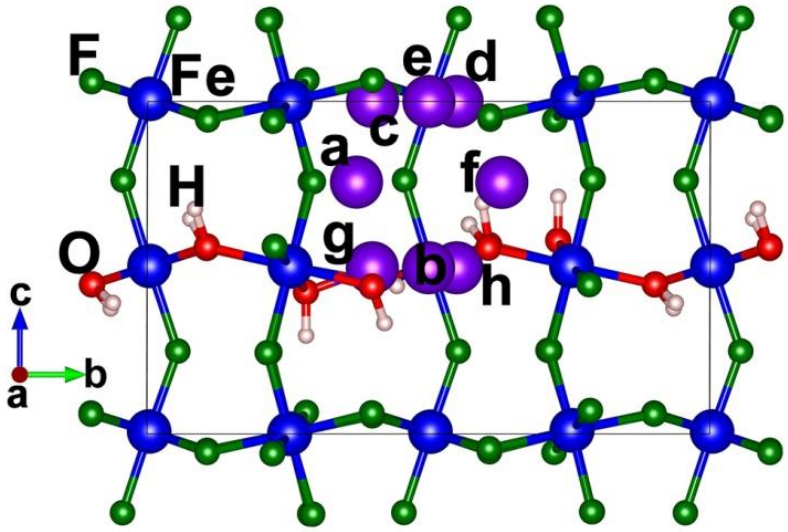

Fig. S11 The Li/Na atomic configurations in the $FeF_{2.2}(OH)_{0.8}$.

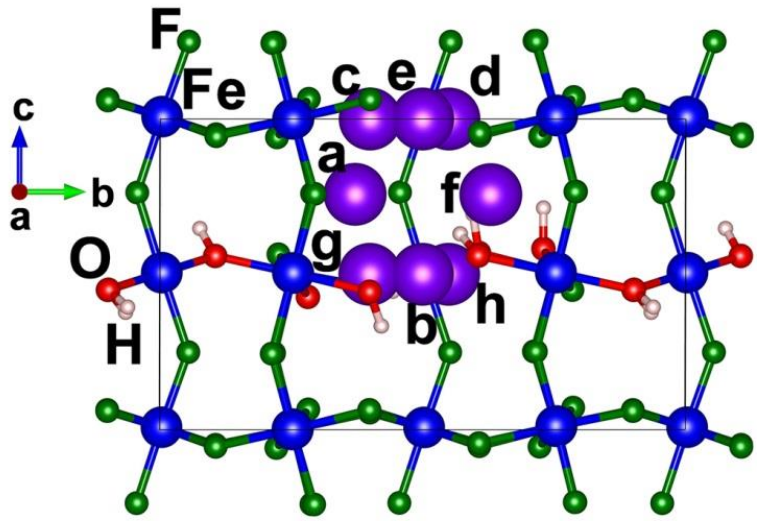

Fig. S12 The Li/Na atomic configurations in the $FeF_{2.2}(OH)_{0.64}O_{0.08}\square_{0.08}$.

Among these sites, the Li/Na optimal occupation sites can be determined by formation energy (E_{form}) defined as follows:

$$E_{\text{form}} = E_{\text{total}} - E_{\text{sub}} - E_i \quad (17)$$

where, E_{total} is the total energy of $FeF_{2.2}(OH)_{0.8}$ or $FeF_{2.2}(OH)_{0.64}O_{0.08}\square_{0.08}$ with Li or Na, E_{sub} is the total energy of $FeF_{2.2}(OH)_{0.8}$ or $FeF_{2.2}(OH)_{0.64}O_{0.08}\square_{0.08}$, the E_i means the total energy of single Li or Na atom. The calculated formation energies (E_{form}) of one Li or Na atom in $FeF_{2.2}(OH)_{0.8}$ and $FeF_{2.2}(OH)_{0.64}O_{0.08}\square_{0.08}$ are summarized in **Table S3**.

Table S3. Formation energies of Li/Na atomic configurations in $FeF_{2.2}(OH)_{0.8}$ and $FeF_{2.2}(OH)_{0.64}O_{0.08}\square_{0.08}$.

sites	$FeF_{2.2}(OH)_{0.8}$ (eV)		$FeF_{2.2}(OH)_{0.64}O_{0.08}\square_{0.08}$(eV)	
	Li	Na	Li	Na
a	-3.07	-2.81	-2.08	-2.11
b	-2.61	-3.24	-2.30	-2.24
c	-2.84	-2.95	-1.77	-2.99
d	-1.70	-2.67	-2.80	-2.24
e	-2.10	-2.61	-2.11	-0.88
f	-2.68	-1.04	-2.03	-1.86
g	-2.97	-3.05	-2.28	-2.76
h	-2.59	-2.83	-2.67	-2.43

As shown in **Table S3**, it should also be noted that the Li and Na both have negative formation energies. Hence, occupation is favorable for these two atoms. Moreover, their strong binding occurs, which indicates Li and Na clusters are difficult to form in $FeF_{2.2}(OH)_{0.8}$ and $FeF_{2.2}(OH)_{0.64}O_{0.08}\square_{0.08}$ and they can be acted as good electrode materials. What's more, by comparison, it is found that Li and Na prefer to occupying a and b sites in the $FeF_{2.2}(OH)_{0.8}$, respectively, with the lowest formation energy (-3.07 eV for Li and -3.24 eV for Na).

Similarly, as for $FeF_{2.2}(OH)_{0.64}O_{0.08}\square_{0.08}$, d and c sites are transferred to the energetically favorite sites for Li or Na atom occupying due to the lowest formation energy (-2.80 eV for Li and -2.99 eV for Na). In general, The binding strength of Na is stronger relative to Li in $FeF_{2.2}(OH)_{0.8}$ and $FeF_{2.2}(OH)_{0.64}O_{0.08}\square_{0.08}$.

8. Thermal stability of $FeF_{2.2}(OH)_{0.8}$ and $FeF_{2.2}(OH)_{0.64}O_{0.08}\square_{0.08}$ with Li/Na occupation

We further analyzed the thermal stability of Li or Na in the pristine or defective structures with AIMD using the NVT ensemble and a Nose-Hoover thermostat at 300K (see **Fig. S13-Fig. S16**). When Li/Na atoms are located in $FeF_{2.2}(OH)_{0.8}$ and $FeF_{2.2}(OH)_{0.64}O_{0.08}\square_{0.08}$, the corresponding total potential energy all reach equilibrium very quickly and fluctuate near the equilibrium (see **Fig. S13**). Li/Na atoms incline to diffuse and other atoms are bound within limits. In order to further clarify clearly the stability of $FeF_{2.2}(OH)_{0.8}$ and $FeF_{2.2}(OH)_{0.64}O_{0.08}\square_{0.08}$, we calculated mean square displacement (MSD)[6, 7] of Li/Na, Fe, F and O atoms in $Li_{0.08}FeF_{2.2}(OH)_{0.8}$, $Li_{0.08}FeF_{2.2}(OH)_{0.64}O_{0.08}\square_{0.08}$, $Na_{0.08}FeF_{2.2}(OH)_{0.8}$ and $Na_{0.08}FeF_{2.2}(OH)_{0.64}O_{0.08}\square_{0.08}$, together with $FeF_{2.2}(OH)_{0.8}$ and $FeF_{2.2}(OH)_{0.64}O_{0.08}\square_{0.08}$ as a reference at 300 K (see **Fig. S14-Fig. S16**). It is obvious that Fe, F and O atoms are bound within limits in $FeF_{2.2}(OH)_{0.8}$ and $FeF_{2.2}(OH)_{0.64}O_{0.08}\square_{0.08}$. Moreover, Fe, F and O atoms still keep excellent structural stabilty with Li/Na insertion. Therefore, $FeF_{2.2}(OH)_{0.8}$ and $FeF_{2.2}(OH)_{0.64}O_{0.08}\square_{0.08}$ both possess excellent thermal stability.

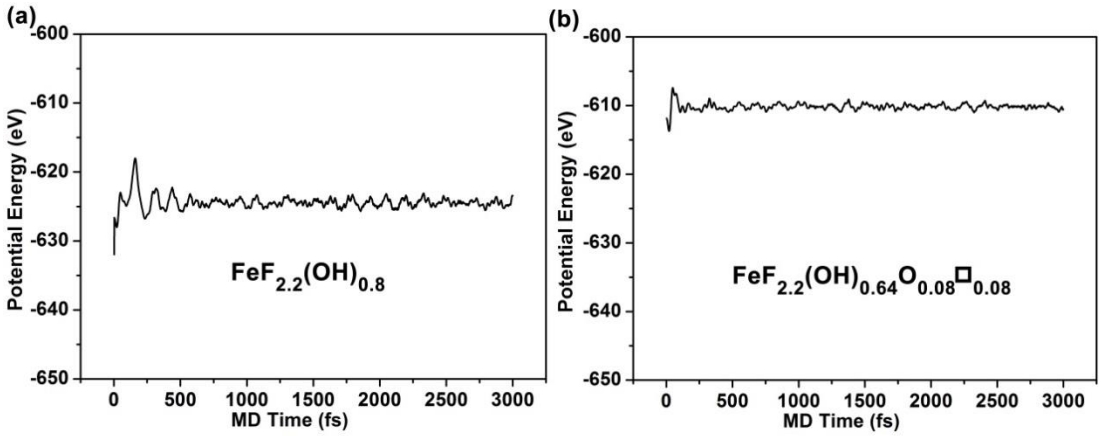

Fig. S13 Total potential energy as a function of MD time at 300 K. (a) $FeF_{2.2}(OH)_{0.8;}$ (b) $FeF_{2.2}(OH)_{0.64}O_{0.08}\square_{0.08}FeF_{2.2}(OH)_{0.8}$.

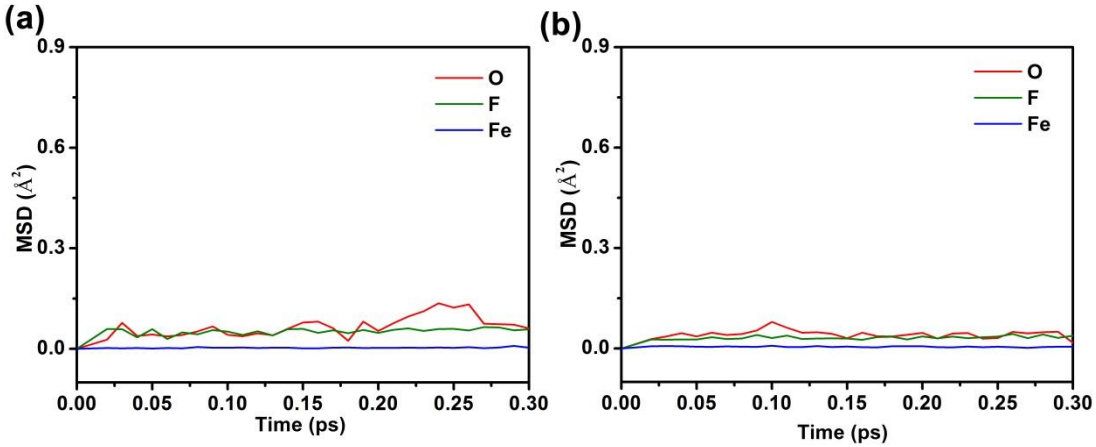

Fig. S14 MSD function of Fe, F and O in $FeF_{2.2}(OH)_{0.8}$ and $FeF_{2.2}(OH)_{0.64}O_{0.08}\square_{0.08}$ at 300 K.

(a) $FeF_{2.2}(OH)_{0.8}$; (b) $FeF_{2.2}(OH)_{0.64}O_{0.08}\square_{0.08}$.

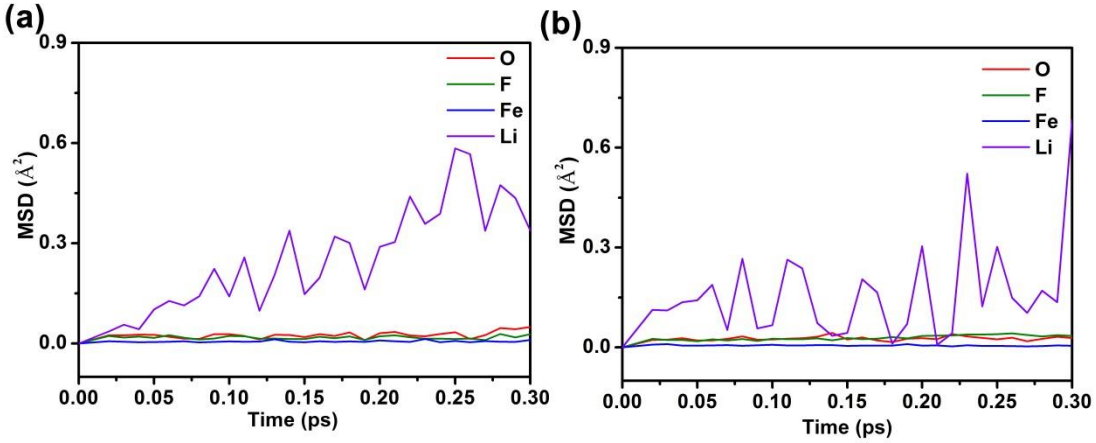

Fig. S15 MSD function of Li, Fe, F and O in $Li_{0.08}FeF_{2.2}(OH)_{0.8}$ and $Li_{0.08}FeF_{2.2}(OH)_{0.64}O_{0.08}\square_{0.08}$ at 300 K.(a) $Li_{0.08}FeF_{2.2}(OH)_{0.8}$;(b)$Li_{0.08}FeF_{2.2}(OH)_{0.64}O_{0.08}\square_{0.08}$.

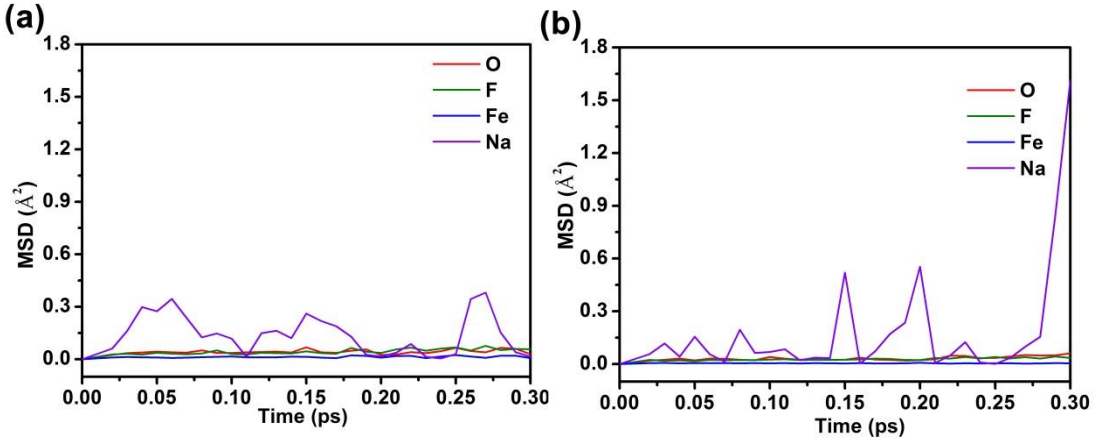

Fig. S16 MSD function of Na, Fe, F and O in $Na_{0.08}FeF_{2.20}(OH)_{0.8}$ and $Na_{0.08}FeF_{2.2}(OH)_{0.64}O_{0.08}\square_{0.08}$ at 300 K.

(a)$Na_{0.08}FeF_{2.2}(OH)_{0.8}$; (b)$Na_{0.08}FeF_{2.2}(OH)_{0.64}O_{0.08}\square_{0.08}$.

9. Stability of $FeF_{2.2}(OH)_{0.8}$ and $FeF_{2.2}(OH)_{0.64}O_{0.08}\square_{0.08}$ with increasing Li/Na concentration

In order to assess stability of $FeF_{2.2}(OH)_{0.8}$ and $FeF_{2.2}(OH)_{0.64}O_{0.08}\square_{0.08}$ with increasing adatom (Li/Na) concentration, we calcluated formation energies of $Li_xFeF_{2.2}(OH)_{0.8}$, $Li_xFeF_{2.2}(OH)_{0.64}O_{0.08}\square_{0.08}$, $Na_xFeF_{2.2}(OH)_{0.8}$ and $Na_xFeF_{2.2}(OH)_{0.64}O_{0.08}\square_{0.08}$ according to the expression as follows (see **Fig. S17**):

$$E_f = \frac{1}{x}[E(M_xFeF_{2.2}(OH)_{0.8-2y}O_y\square_y) - FeF_{2.2}(OH)_{0.8} - xE_M] \quad (18)$$

As shown in **Fig. S17**, it is obvious that the formation energies of these four compounds increase with increasing Li/Na concentrations, which indictates that their stability decreases with increasing adatom (Li/Na) concentrations.

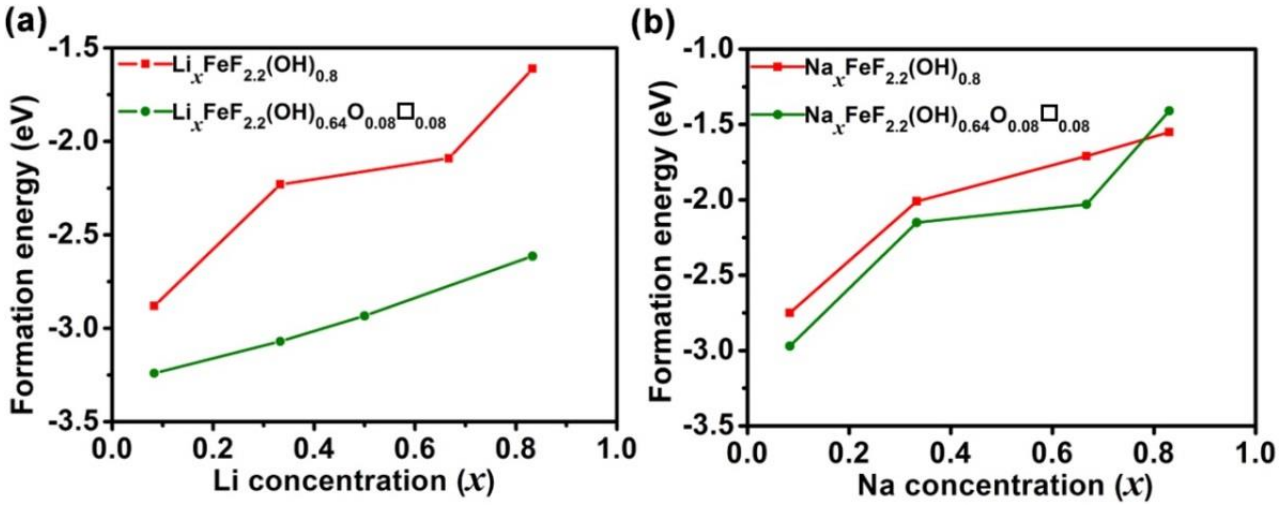

Fig. S17 (a) The formation energies of $Li_xFeF_{2.2}(OH)_{0.8}$ and $Li_xFeF_{2.2}(OH)_{0.64}O_{0.08}\square_{0.08}$ as a function of Li concentration (x); (b) The formation energies of $Na_xFeF_{2.2}(OH)_{0.8}$ and $Na_xFeF_{2.2}(OH)_{0.64}O_{0.08}\square_{0.08}$ as a function of Na concentration (x).

10. Li /Na diffusion process in $FeF_{2.2}(OH)_{0.8}$ and $FeF_{2.2}(OH)_{0.64}O_{0.08}\square_{0.08}$

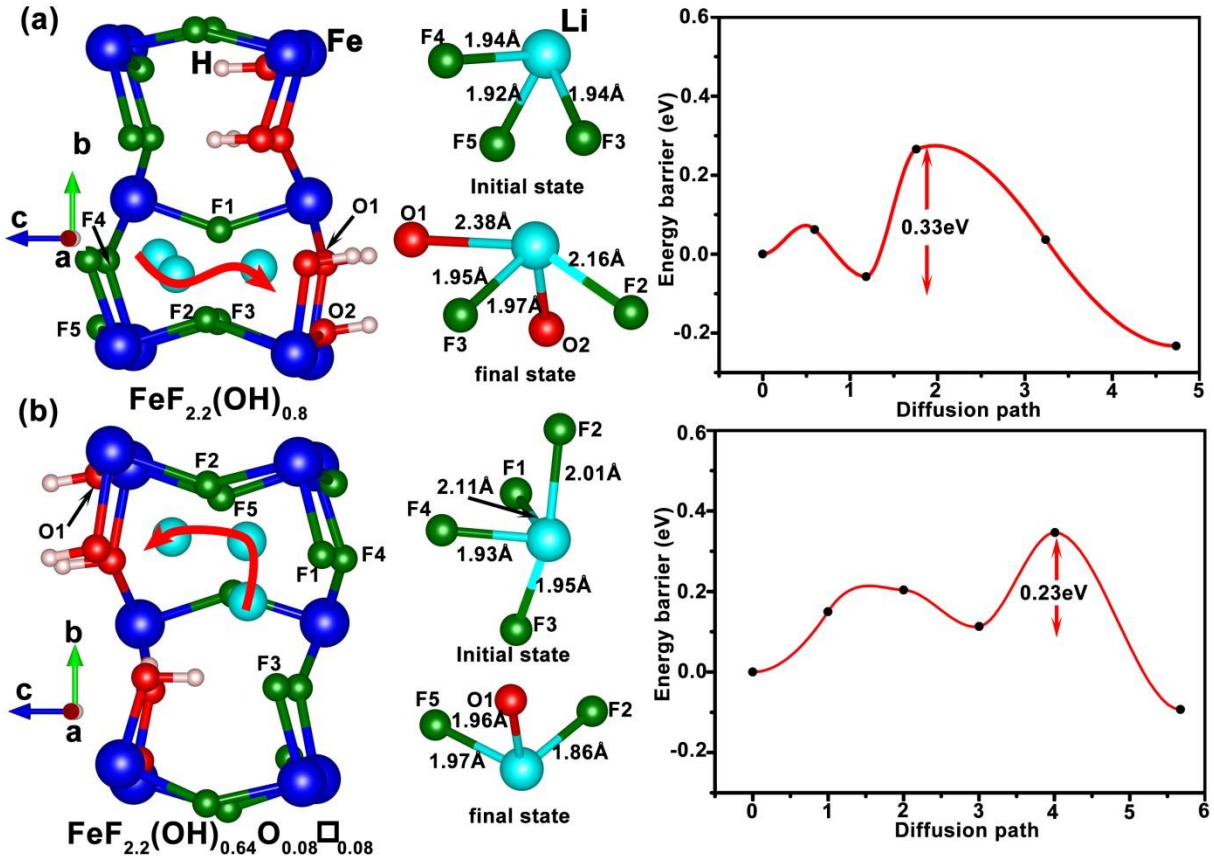

Fig. S18 The optimal migration paths, initial states, final states and energy barriers of Li diffusion in (a) $FeF_{2.2}(OH)_{0.8}$ (b) $FeF_{2.2}(OH)_{0.64}O_{0.08}\square_{0.08}$.

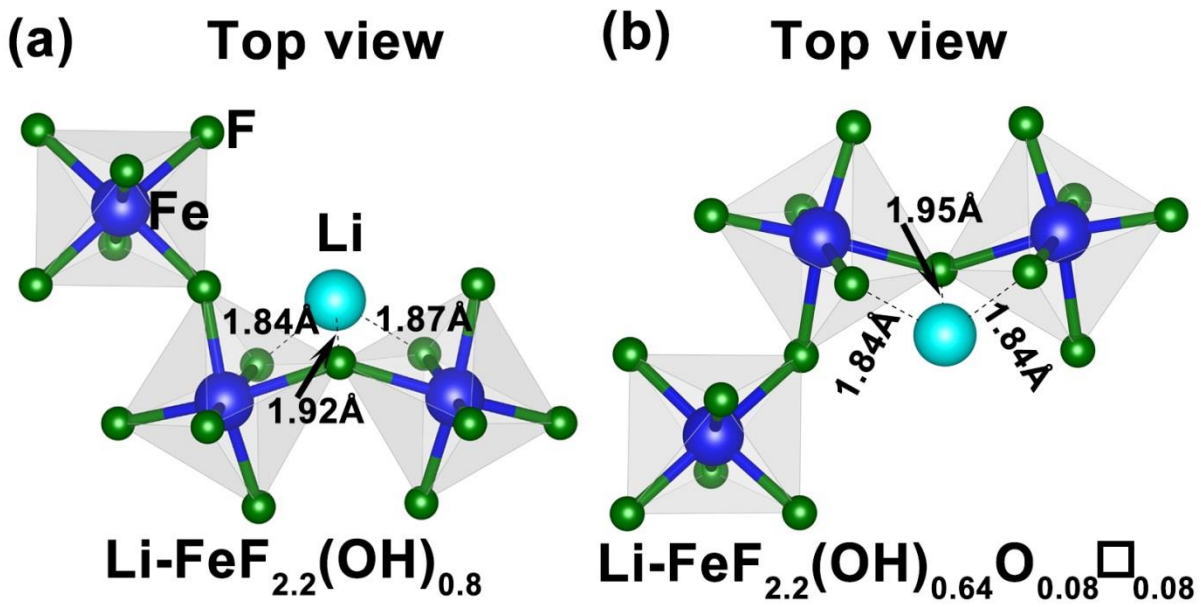

Fig. S19 The transition state structures of (a) $FeF_{2.2}(OH)_{0.8}$ (b) $FeF_{2.2}(OH)_{0.64}O_{0.08}\square_{0.08}$.

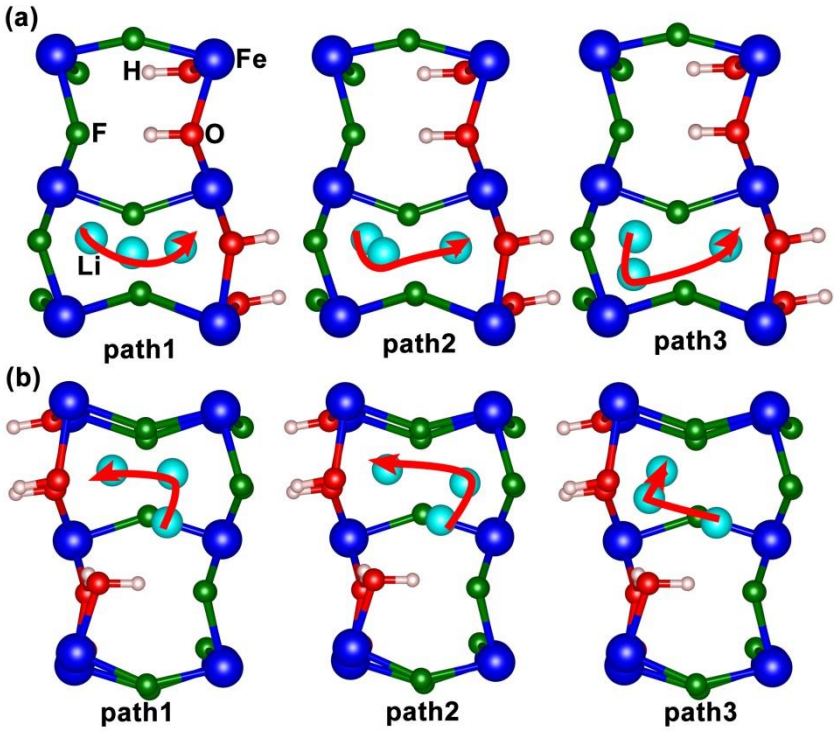

Fig. S20 Three different migration paths (path1, path2 and path3) for Li in (a) $FeF_{2.2}(OH)_{0.8}$ and (b) $FeF_{2.2}(OH)_{0.64}O_{0.08}\square_{0.08}$.

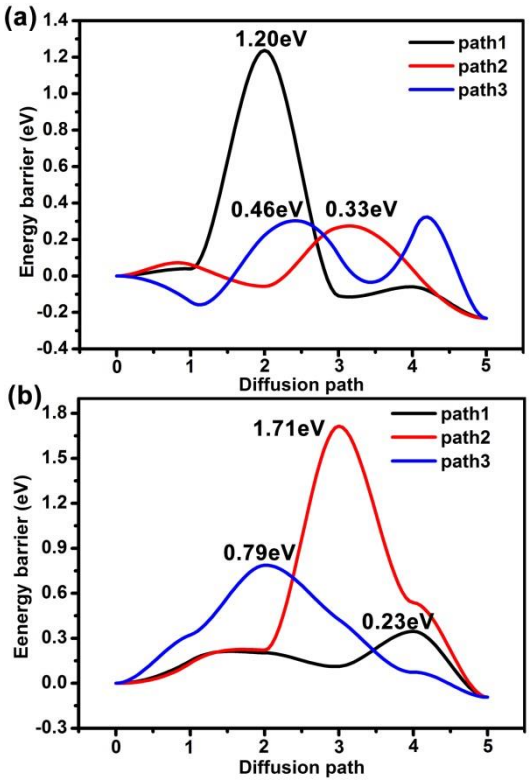

Fig. S21 The Li diffusion energy barriers along three different paths (path1, path2 and path3) (a) $FeF_{2.2}(OH)_{0.8}$ (b) $FeF_{2.2}(OH)_{0.64}O_{0.08}\square_{0.08}$.

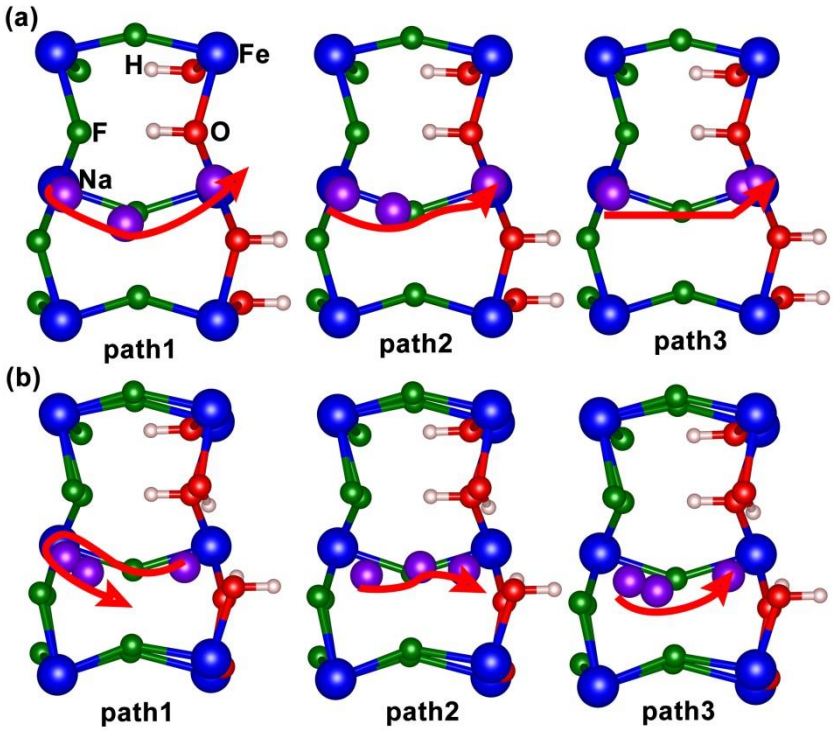

Fig. S22 Three different migration paths (path1, path2 and path3) for Na in (a) $FeF_{2.2}(OH)_{0.8}$ and (b) $FeF_{2.2}(OH)_{0.64}O_{0.08}\square_{0.08}$.

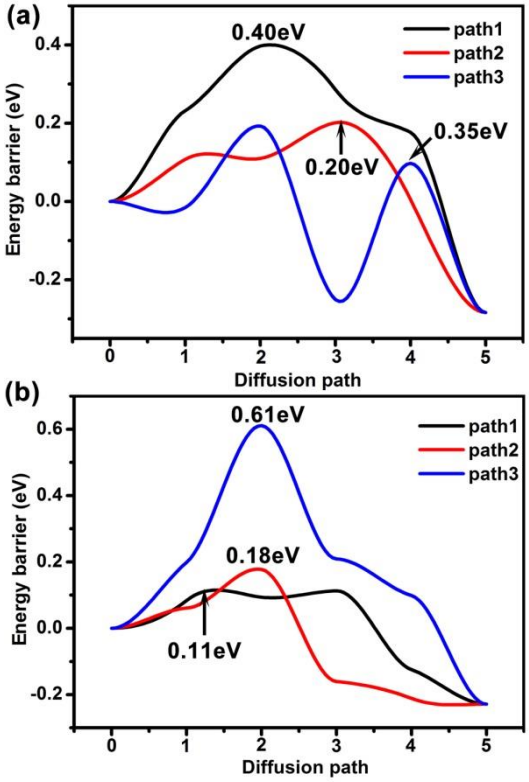

Fig. S23 The Na diffusion energy barriers along three different paths (path1, path2 and path3) (a) $FeF_{2.2}(OH)_{0.8}$; (b) $FeF_{2.2}(OH)_{0.64}O_{0.08}\square_{0.08}$.

Table S4. Path lengths, energy barriers, diffusion coefficient and ionic conductivity of Li/Na along path1, path2 and path3 in $FeF_{2.2}(OH)_{0.8}$ and $FeF_{2.2}(OH)_{0.64}O_{0.08}\square_{0.08}$.

structure	Path	Path lengths (Å)	energy barrier (eV)	diffusion coefficient ($cm^2\ s^{-1}$)	Ionic conductivity ($S\ cm^{-1}$)
Li-$FeF_{2.2}(OH)_{0.8}$	Path1	1.85	1.20	2.58×10^{-25}	9.64×10^{-22}
	Path2	0.57	0.33	2.68×10^{-10}	1×10^{-6}
	Path3	4.76	0.46	7.49×10^{-11}	2.80×10^{-7}
Na-$FeF_{2.2}(OH)_{0.8}$	Path1	2.68	0.40	3.03×10^{-10}	1.13×10^{-6}
	Path2	5.14	0.20	5.43×10^{-6}	2.03×10^{-2}
	Path3	1.71	0.35	1.03×10^{-9}	3.85×10^{-6}
Li-$FeF_{2.2}(OH)_{0.64}O_{0.08}\square_{0.08}$	Path1	1.00	0.23	1.38×10^{-7}	5.16×10^{-4}
	Path2	2.53	1.79	5.96×10^{-33}	2.23×10^{-29}
	Path3	3.64	0.79	3.61×10^{-17}	1.35×10^{-13}
Na-$FeF_{2.2}(OH)_{0.64}O_{0.08}\square_{0.08}$	Path1	1.40	0.11	1.84×10^{-5}	6.88×10^{-2}
	Path2	2.43	0.18	2.84×10^{-6}	1.06×10^{-2}
	Path3	2.26	0.61	2.90×10^{-14}	1.08×10^{-10}

References

1. S. B. Zhang and J. E. Northrup, *Phys. Rev. Lett.* 1991**, 67**, 2339-2342.
2. M. W. Chase, *Journal of Physical and Chemical Reference Data* 1998, **9**.
3. L. Bjaalie, A. Janotti, K. Krishnaswamy and C. G. V. D. Walle, *Phys. Rev. B* 2016**, 93**, 115316.
4. Q. Cai, J.-g. Wang, Y. Wang and D. Mei, *J. Phys. Chem. C* 2016**, 120**, 19087-19096.
5. M. Shishkin, T. Ziegler, *Surf. Sci.* 2012**, 606**, 1078-1087.
6. G. Tao, *J. Phys. Chem. C*, 2016, **120**, 6938-6952.
7. J. B. Varley, K. Kweon, P. Mehta, P. Shea, T. W. Heo, T. J. Udovic, V. Stavila and B. C. Wood, *ACS Energy Lett.*, 2016, **2**, 250-255.